Tensile Rupture of Rectangular Hollow Section Flexural Members with Holes In the Tension Flange

BRENDAN RICHARDS and KYLE TOUSIGNANT

ABSTRACT

An evaluation of the AISC *Specification* Section F13.1 provisions for the reduction in strength of beams and girders with holes in the tension flange is performed. Twelve simply supported rectangular hollow section (RHS)-to-RHS splice connections with variations in RHS shape, number of bolts, and bolting arrangement are tested under monotonic four-point bending, and net-section rupture (in the tension flange) is achieved. The results demonstrate that, for RHS members, the current AISC *Specification* Section F13.1 provisions are vastly conservative. The current results are combined with the previous data from 138 tests on wide-flange girders with holes in the tension flange, and a new nominal flexural strength (M_n) equation is developed using net section properties. The new equation is shown to increase the accuracy of M_n predictions and reduce scatter in the predicted results. A reliability analysis is performed to demonstrate that the new approach provides acceptable levels of reliability when compared to the target reliability index of 4.0 specified in Chapter B of the *Specification* commentary.

KEYWORDS: rectangular hollow sections, flexural members, beams, girders, tensile rupture, bolts.

INTRODUCTION

The current expression in AISC *Specification for Structural Steel Buildings* Section F13.1 (2022a), hereafter referred to as the AISC *Specification*, for the nominal flexural strength, M_n, of members (i.e., beams and girders) with holes in the tension flange covers rolled or built-up shapes and cover-plated beams with holes, proportioned on the basis of flexural strength of the gross section. According to this section, M_n—for the limit state of tensile rupture of the tension flange—is calculated when

$$F_u A_{fn} < Y_t F_y A_{fg} \tag{1}$$

in which case,

$$M_n = \frac{F_u A_{fn}}{A_{fg}} S_x \tag{2}$$

where F_u and F_y are the specified minimum tensile and yield strengths, respectively, given in Table 2-4 of the AISC *Steel Construction Manual* (2023); A_{fn} and A_{fg} are the net and gross area of the tension flange, respectively; S_x is the minimum elastic section modulus taken about the x-axis; and $Y_t = 1.0$ for $F_y/F_u \le 0.8$ and 1.1 otherwise. When Equation 1 is not met—that is, when $Y_t F_y A_{fg} \le F_u A_{fn}$—the limit state of rupture does not apply.

Equation 2 reduces the flexural strength of the cross section as a function of A_{fn}/A_{fg} to provide an acceptable margin of safety against rupture of the tension flange; however, its predictions are well-known to be conservative for plastic design/compact sections (which, in the absence of holes, can develop the plastic moment, M_p). With an interest in developing field-bolted connections for hollow structural sections (HSS) members, the over-conservatism of AISC *Specification* Section F13.1—for all members—is a salient issue.

AISC *Specification* Section F13.1 was developed from experiments on W-shape and T-shaped cross sections (Dexter and Altstadt, 2004; Yuan et al., 2004), with scant research done to assess its overall reliability and applicability to other cross-sectional shapes. This study addresses that gap by evaluating Section F13.1 in a probabilistic manner, in relation to rectangular hollow section (RHS) members with holes in the tension flange. The design of these connections—namely, RHS-to-RHS bolted splice connections for flexure—is required by the AISC *Seismic Provisions for Structural Steel Buildings* (2022b) for (beam-)columns in intermediate moment frames (IMFs), special moment frames (SMFs), and special truss moment frames (STMFs).

This paper presents an experimental program to assess the applicability of AISC *Specification* Section F13.1 (2022a) to RHS-to-RHS bolted splice connections, a comparison(s) of the results to those from 138 previous numerical and experimental tests on W-shaped cross sections, and a reliability assessment. The results of this research support a recommendation to modify the provision to improve its accuracy and economy.

Brendan Richards, Ph.D. Candidate, Department of Civil & Resource Engineering, Dalhousie University, Halifax, NS, Canada.
Email: brendan.richards@dal.ca

Kyle Tousignant, Associate Professor, Department of Civil & Resource Engineering, Dalhousie University, Halifax, NS, Canada.
Email: kyle.tousignant@dal.ca (corresponding)

Paper No. 2025-03R

Table 1. RHS and Plate Dimensions and Properties										
	RHS							Plate(s)		
No.	Shape	H (in.)	B (in.)	t_{des} (in.)	A_{fg}* (in.^{2})	S_x (in.^{3})	Z_x (in.^{3})	Dimensions	B_p (in.)	t_p (in.)
1	6×6×¼	6.00	6.00	0.233	1.18	9.52	11.2	4⅞×⅞	4.88	0.88
2	7×7×¼	7.00	7.00	0.233	1.41	13.3	15.5	5⅞×¾	5.88	0.75
3	7×7×¼	7.00	7.00	0.233	1.41	13.3	15.5	5⅞×¾	5.88	0.75
4	8×8×½	8.00	8.00	0.465	2.86	31.2	37.5	5¾×1⅝	5.75	1.63
5	8×8×⅝	8.00	8.00	0.581	3.30	36.5	44.7	5^3⁄$_{16}$×⅞	5.19	0.88
6	8×8×⅝	8.00	8.00	0.581	3.30	36.5	44.7	5^3⁄$_{16}$×⅞	5.19	0.88
7	10×8×½	10.00	8.00	0.465	2.86	42.7	51.9	5¾×1⅞	5.75	1.88
8	12×6×¼	12.00	6.00	0.233	1.18	25.2	31.1	4⅞×1⅜	4.88	1.38
9	12×8×⅜	12.00	8.00	0.349	2.30	43.7	52.9	6^5⁄$_{16}$×1⅝	6.31	1.63
10	12×8×⅜	12.00	8.00	0.349	2.30	43.7	52.9	6^5⁄$_{16}$×1¾	6.31	1.75
11	7×5×⅜	7.00	5.00	0.349	1.26	14.1	17.5	3^5⁄$_{16}$×1¾	3.31	1.75
12	7×5×⅜	7.00	5.00	0.349	1.26	14.1	17.5	3^5⁄$_{16}$×1¾	3.31	1.75

* Note: Determined in accordance with AISC *Specification* using $A_{fg} = (B - 4t_{des})t_{des}$.

Table 2. Bolt Nominal Properties									
No.	Size	Grade	n_b	n_r	d (in.)	d_h (in.)	s (in.)	g (in.)	l_c (in.)
1	¾×2¾	A490	24	2	0.750	0.813	3.38	2.00	3.38
2	¾×2¾	A490	32	1	0.750	0.813	3.00	—	3.00
3	⅞×2¾	A490	28	1	0.875	0.938	3.00	—	3.00
4	⅞×3¾	A490	40	1	0.875	0.938	3.00	—	3.00
5	⅞×3	A325	24	1	0.875	0.938	3.00	—	3.00
6	¾×3¼	A490	32	1	0.750	0.813	3.00	—	3.00
7	⅞×4	A490	44	1	0.875	0.938	3.00	—	3.00
8	¾×3	A490	40	2	0.750	0.813	3.50	2.00	3.50
9	¾×3¾	A325	64	2	0.750	0.813	3.00	3.00	3.00
10	1×4	A325	40	2	1.000	1.063	4.00	3.00	4.00
11	⅞×3¼	A490	24	1	0.875	0.938	3.00	—	3.00
12	¾×3¼	A325	32	1	0.750	0.813	3.00	—	3.00

SCOPE OF TESTING

Overview of Connections

For the current study, 12 RHS-to-RHS bolted splice connections comprised of two RHS members, finished to bear and bolted together by means of internal splice plates, were designed to fail by rupture of the tension flange under strong-axis bending. The 12 connections were designed with varying ratios of A_{fn}/A_{fg} and S_x and, as a result, varied the net elastic section modulus taken about the axis of bending, the plastic section modulus taken about the x-axis, and the net plastic section modulus taken about the axis of bending (S_n, Z_x, and Z_n, respectively). These variations were achieved by using RHS members with different shapes and connections with different numbers of bolts, bolt sizes, and bolt arrangements, within the limits outlined in AISC *Specification* Sections J3.3 and J3.4. Table 1 summarizes the RHS shapes for each connection and provides nominal values of the members' overall height, H; overall width, B; design wall thickness, t_{des} (= $0.93t_{nom}$, where t_{nom} = nominal wall thickness); and gross-section properties, A_{fg}, S_x, and Z_x. The splice-plate cross-sectional dimensions, including width, B_p, and thickness, t_p, are also given. Table 2 provides the bolt designations (i.e., $d \times l_{bolt}$, where d is the nominal diameter of the fastener and l_{bolt} is the nominal bolt

length); bolt grades; total number of bolts per connection, n_b; number of bolts per row, n_r; diameter of the bolt hole, d_h; longitudinal center-to-center spacing (pitch) of two consecutive bolt holes, s; transverse center-to-center spacing (gage) between fastener gage lines, g; and clear distance, in the direction of the force, between the edge of the hole and the edge of the material, l_c, for each connection. A detail/schematic of a typical test connection is also presented, in Figure 1, where A_{net} is the net-effective area subjected to tension under pure flexure, shown shaded in Figure 1(a).

The RHS members were dual certified to ASTM A500 Grade B and C with a minimum F_y = 50 ksi and a minimum F_u = 62 ksi (AISC, 2022a; ASTM, 2021). The internal splice plates conformed to CAN/CSA-G40.20/G40.21 Grade 350W with a minimum F_y = 51 ksi and a minimum F_u = 65 ksi (AISC, 2022a; CSA, 2023). As shown in Table 2, the bolts conformed to ASTM F3125/F3125M Grade A325 or Grade A490 with nominal shear stress, F_{nv}, of 68 ksi or 84 ksi, respectively, with threads excluded from the shear plane (AISC, 2022a; ASTM, 2023). All bolts were installed in drilled holes with $d_h = d + 1/16$ in.

Design Process for Rupture-Critical Tests

To ensure that rupture of the RHS tension flange governed the connection strength, the other possible limit states for the RHS (i.e., gross-section yielding and block shear), splice plates (tensile rupture, plate buckling and block shear), and bolts (bearing, tear-out, and shear), were designed to have an axial resistance equal to or greater than a force resulting from bending of $A_{net}F_u$.

For Specimens 5 and 6 (which utilized HSS 8×8×⅝ members), the geometric limitations and necessary bolt configurations precluded this design approach, so an alternative method was used. In these cases, the connections were designed so that all other limit state capacities exceeded a force from bending of $1.15A_{fg}F_y$. This was justified by 138 past experimental and numerical tests on W-shape sections that failed by tensile rupture of the tension flange in which the ultimate bending moments were 12% greater, on average, than the nominal plastic bending moment resistance of the gross section(s).

Because test specimens were designed to fail by rupture of the tension flange (of the RHS), tensile coupon (TC) tests were conducted on the RHS material(s). For each heat of material, three TCs taken from mid-width of the RHS flats (excluding the face with the weld seam) were tested in accordance with ASTM E8/E8M-22 (ASTM, 2022). Table 3 summarizes the average results of the tests for each member, including the modulus of elasticity, E; measured values of F_y and F_u; and the yield, ultimate, and rupture strains (ε_y, ε_u, and ε_r, respectively).

The geometric properties of the RHS (i.e., H, B, and t, where t is the measured wall thickness) were also measured, and the gross-section properties (i.e., A_{fg}, S_x, and Z_x) were recomputed assuming an outside corner radius of 2.0t (AISC, 2022a). The measured geometric properties of the RHS and calculated gross section properties are shown in Table 4.

To facilitate tensile rupture of the tension flange of the RHS, portions of members outside the connection region (i.e., beyond the ends of the splice plates) were reinforced using material taken from the elastic shear spans of previously tested specimens. The reinforcement was applied to the compression flange and part of each web, as shown in Figure 2 (where B_s is the stiffener plate overall width, H_s is the stiffener plate overall height, t_s is the stiffener plate thickness, and A_{gc} is the gross area subjected to compression, shown shaded). The measured geometric properties of

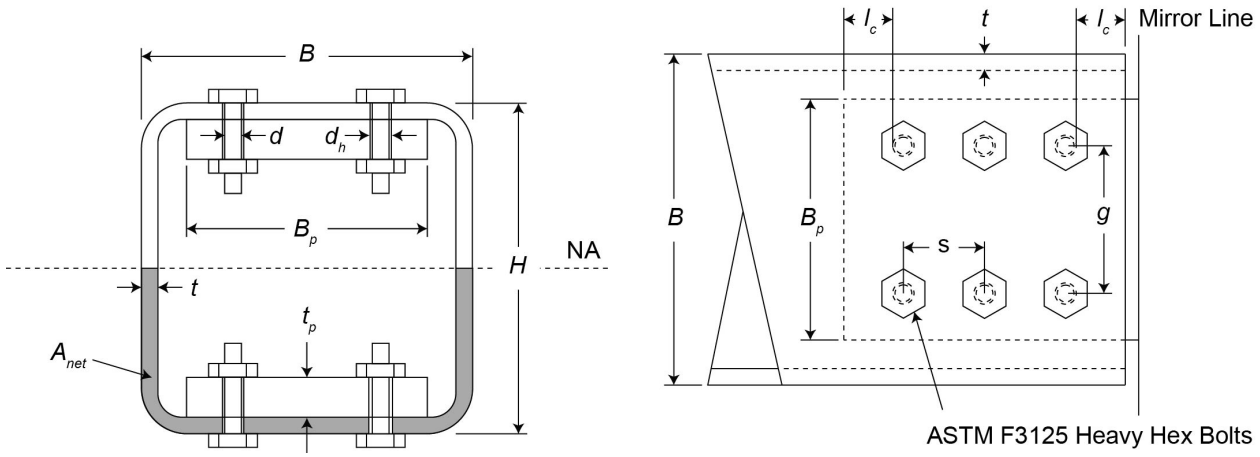

(a) Cross section *(b) Plan view*

Fig. 1. Test connection schematic.

Table 3. Measured RHS Material Properties							
No.	Shape	E (ksi)	F_y (ksi)	F_u (ksi)	ε_y%	ε_u%	ε_r%
1	6×6×¼	32457	56.2	71.8	0.351	16.3	29.1
2	7×7×¼	32192	63.2	75.2	0.359	14.4	26.9
3	7×7×¼	32192	63.2	75.2	0.359	14.4	26.9
4	8×8×½	28326	50.7	66.3	0.366	14.3	29.4
5	8×8×⅝	29117	60.9	72.1	0.378	10.6	28.8
6	8×8×⅝	29117	60.9	72.1	0.378	10.6	28.8
7	10×8×½	31141	50.7	68.4	0.356	14.5	31.2
8	12×6×¼	28853	56.5	72.0	0.366	15.2	25.7
9	12×8×⅜	32764	62.2	75.6	0.354	13.1	28.9
10	12×8×⅜	32764	62.2	75.6	0.354	13.1	28.9
11	7×5×⅜	27984	60.9	73.2	0.413	12.1	29.1
12	7×5×⅜	27984	60.9	73.2	0.413	12.1	29.1

the stiffeners and the locations of the geometric centroid, y, in the stiffened region of the connection—measured from the bottom of the RHS (Figure 2)—are given in Table 4.

The predicted (nominal) strength for each limit state was calculated in accordance with the AISC *Specification* using the measured properties of the RHS (Tables 3 and 4) and the nominal properties of the plates and bolts (Tables 1 and 2). The latter, conservative, approach was only used for noncritical limit states to ensure they did not govern. The predicted axial strengths are summarized in Table 5, which assumes each element to be loaded by a force couple from bending acting through its geometric center. Table 6 summarizes the predicted flexural strengths, which were determined by multiplying the axial strength(s)/forces in Table 5 by their corresponding lever arm(s). The limit state governing each test is indicated by a bold value in each corresponding row, and tensile rupture of the tension flange was predicted to govern, under flexure, in 10 out of 12 connections. References to the appropriate sections of the AISC *Specification* for each limit state are also given, and Figures 3(a) and (b) illustrate the block-shear failure patterns considered (in which A_{gv} is the gross area subject to shear, A_{nv} is the net area subject to shear, and A_{nt} is the net area subject to tension).

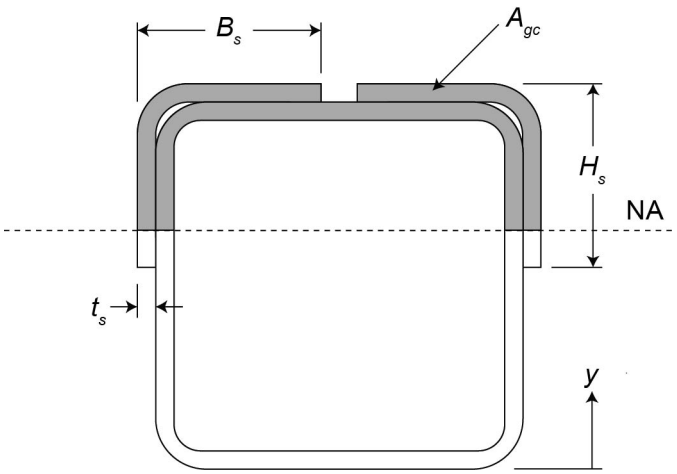

Fig. 2. Stiffened cross section.

Table 4. Measured Dimensions and Properties

No.	RHS							Stiffener			
	Shape	H (in.)	B (in.)	t (in.)	A_{fg} (in.^{2})	S_x (in.^{3})	Z_x (in.^{3})	H_s (in.)	B_s (in.)	t_s (in.)	y (in.)
1*	6×6×¼	5.94	5.98	0.226	1.15	9.16	10.8	—	—	—	2.97
2	7×7×¼	7.01	7.01	0.240	1.45	13.7	16.0	2.97	2.99	0.226	5.13
3	7×7×¼	7.01	7.01	0.240	1.45	13.7	16.0	3.50	3.50	0.240	5.29
4	8×8×½	8.03	8.03	0.457	2.84	31.0	37.3	2.54	3.52	0.342	6.20
5	8×8×⅝	8.07	8.07	0.575	3.32	37.0	45.2	4.02	4.02	0.457	5.69
6	8×8×⅝	8.07	8.07	0.575	3.32	37.0	45.2	4.04	4.04	0.575	6.14
7	10×8×½	10.04	8.07	0.453	2.84	42.4	51.4	4.04	4.04	0.575	8.15
8	12×6×¼	12.01	6.02	0.228	1.16	24.8	30.6	5.02	3.22	0.453	9.36
9	12×8×⅜	12.01	8.07	0.338	2.27	42.9	51.9	6.00	3.01	0.228	7.74
10	12×8×⅜	12.01	8.07	0.338	2.27	42.9	51.9	6.00	4.04	0.338	8.56
11	7×5×⅜	7.05	5.08	0.342	1.27	14.2	17.5	3.50	2.50	0.240	4.83
12	7×5×⅜	7.05	5.08	0.342	1.27	14.2	17.5	3.52	2.54	0.342	5.09

* Note: Unreinforced.

Table 5. Predicted Axial Strength(s) (kips)

No.	RHS				Plate(s)				Bolts		
	F_uA_{net}	$1.15A_{fg}F_y$	F_yA_{gc}	Block Shear*	Tensile Rupture	Buckling	Block Shear* (Pattern 1)	Block Shear* (Pattern 2)	Bearing	Tear-Out	Shear
	AISC *Specification* Section										
	J4.1	J4.1	J4.4	J4.3	J4.1	J4.4	J4.3	J4.3	J3.11	J3.11	J3.7
1	149	—	**142**	173	184	247	619	669	199	392	223
2	217	—	**272**	—	247	256	—	—	282	480	297
3	**215**	—	301	—	241	256	—	—	288	400	353
4	**391**	—	452	—	509	542	—	—	783	949	505
5	—	232	668	—	**242**	263	—	—	592	791	245
6	—	232	729	—	**249**	263	—	—	676	1103	240
7	**464**	—	632	—	587	625	—	—	854	1066	555
8	**250**	—	395	289	289	389	1588	1667	335	678	371
9	**429**	—	510	600	494	595	2485	2520	795	1361	481
10	**417**	—	599	514	474	641	2294	2332	663	1163	534
11	**238**	—	315	—	269	336	—	—	352	478	303
12	**241**	—	344	—	284	336	—	—	402	666	297

* Note: See Figure 3 for block-shear failure patterns.

Table 6. Predicted Flexural Strength(s) (kip-ft)											
	RHS				Plate(s)				Bolts		
	F_uA_{net}	$1.15A_{fg}F_y$	F_yA_{gc}	Block Shear*	Tensile Rupture	Buckling	Block Shear* (Pattern 1)	Block Shear* (Pattern 2)	Bearing	Tear-Out	Shear
	AISC *Specification* Section										
No.	J4.1	J4.1	J4.4	J4.3	J4.1	J4.4	J4.3	J4.3	J3.11	J3.11	J3.7
1	49	—	**50**	83	71	95	238	257	91	179	102
2	88	—	**107**	—	119	123	—	—	154	261	161
3	**87**	—	115	—	116	123	—	—	157	217	192
4	**175**	—	205	—	233	248	—	—	465	563	299
5	—	145	296	—	**122**	133	—	—	341	456	142
6	—	145	320	—	**125**	133	—	—	390	636	139
7	**253**	—	318	—	355	378	—	—	650	811	423
8	**151**	—	221	287	245	330	1347	1413	322	652	357
9	**273**	—	328	592	399	481	2010	2038	751	1285	454
10	**260**	—	370	507	379	512	1832	1862	626	1098	504
11	**87**	—	116	—	104	129	—	—	187	253	161
12	**88**	—	124	—	109	129	—	—	213	353	157

* Note: See Figure 3 for block-shear failure patterns.

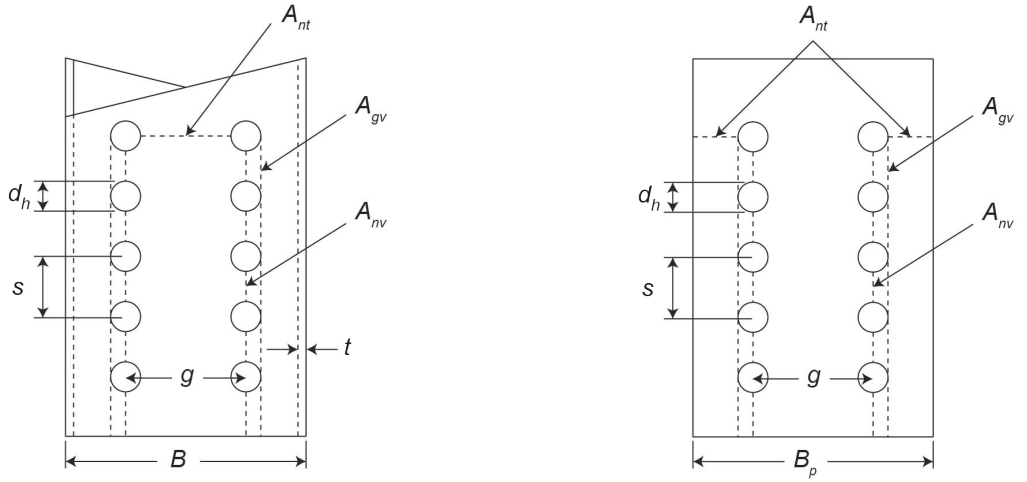

(a) Block shear failure pattern 1 (RHS and splice plate) *(b) Block shear failure pattern 2 (splice plate only)*

Fig. 3. Block shear failure patterns.

Testing Arrangement, Instrumentation, and Loading

Testing Arrangement

Each test specimen was designed with an overall length, L, of 13 ft. 2 in. (12 ft. 10 in. between centerlines of support), with a moment (or shear-free) span of 6 ft. 8 in. that included the connection (Figure 4). They were tested under four-point bending transferred by a W14×53 stiffened spreader beam that was pointed-loaded, at mid-span, by a 225-kip capacity, displacement-controlled, MTS actuator. The specimens were supported at each end by steel rollers atop several layers of blocking (used for elevation control). Web doubler plates ⅝ in. thick were also provided at the load-application and reaction points to prevent web instability.

Instrumentation

To determine the utilization of the cross sections, strain distributions around the perimeter of each RHS were measured using eight linear strain gages (SGs), equidistantly spaced through the RHS web, on the RHS corners, and on half of the tension flange, shown in Figure 5(a). As shown in Figure 5(b), the SGs were placed approximately 1.3 in. from the centerline of the critical net section for consistency in avoiding conflict with the varying bolt-head diameters. Figure 6 shows the three 24-in. string potentiometers (SPs) and two linear variable displacement transducers (LVDTs) used to measure beam displacements. The SPs were placed at mid-span and 3 ft. 4 in. in either direction. The LVDTs were placed at the supports to measure rigid-body movement.

Loading

Displacement-controlled loads were applied at an average rate of 0.2 in./min. to generate applied moments in the constant-moment region. The applied moment, M_a, was determined based on statics, using the specimen geometry and the load applied by the actuator (as measured by an in-line load cell). All data (from the SGs, SPs, LVDTs, and load cell) were recorded by a data acquisition (DAQ) system (see Figure 6) at a rate of 1 Hz.

EXPERIMENTAL RESULTS

Specimens 3, 4, and 7–12 exhibited the desired failure mode of RHS tension flange rupture, as shown typically (for Specimens 3, 4, 10 and 11) in Figure 7. Figure 8 presents typical plots of the measured strains around the cross section(s) at 50%, 75%, 90%, and 95% of the ultimate moment, M_u, and Figure 9 shows beam displacement profiles at the corresponding intervals.

The measured strains in the tension flange(s) at the critical net-section indicates a strain distribution at the onset of fracture (approximately $0.90M_u$), which extends beyond the flat portion of the tension flange (i.e., gages 1–3) and into the corner (i.e., gage 4), after which there is a loss of stiffness caused by incipient fracture near the bolt hole(s) (i.e., gages 1 and 2). When this happens, the stress/strain redistributes from the center of the tension flange out toward the stiffer corner region(s) (i.e., gages 3 and 4). This is illustrated by the typical sharp increase(s) in strain in gages 3 and 4 at $0.95M_u$.

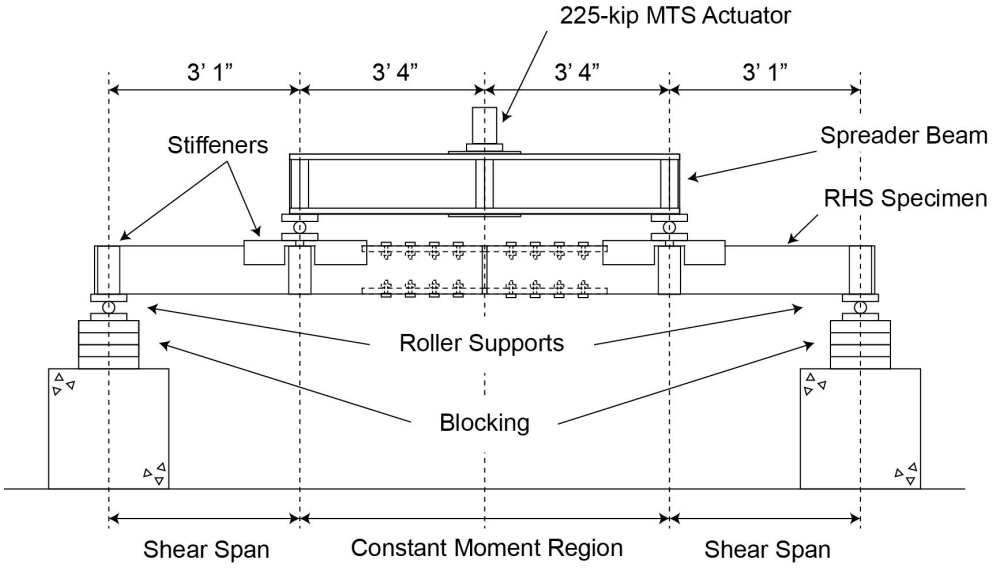

Fig. 4. Testing arrangement.

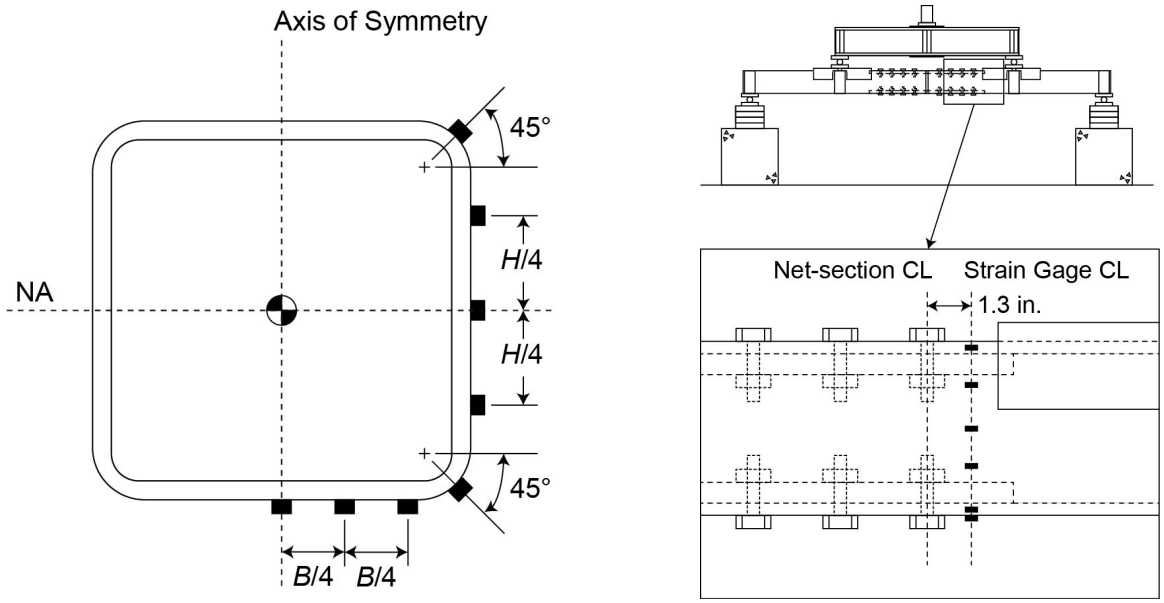

(a) Cross section *(b) Elevation*

Fig. 5. Strain gage locations.

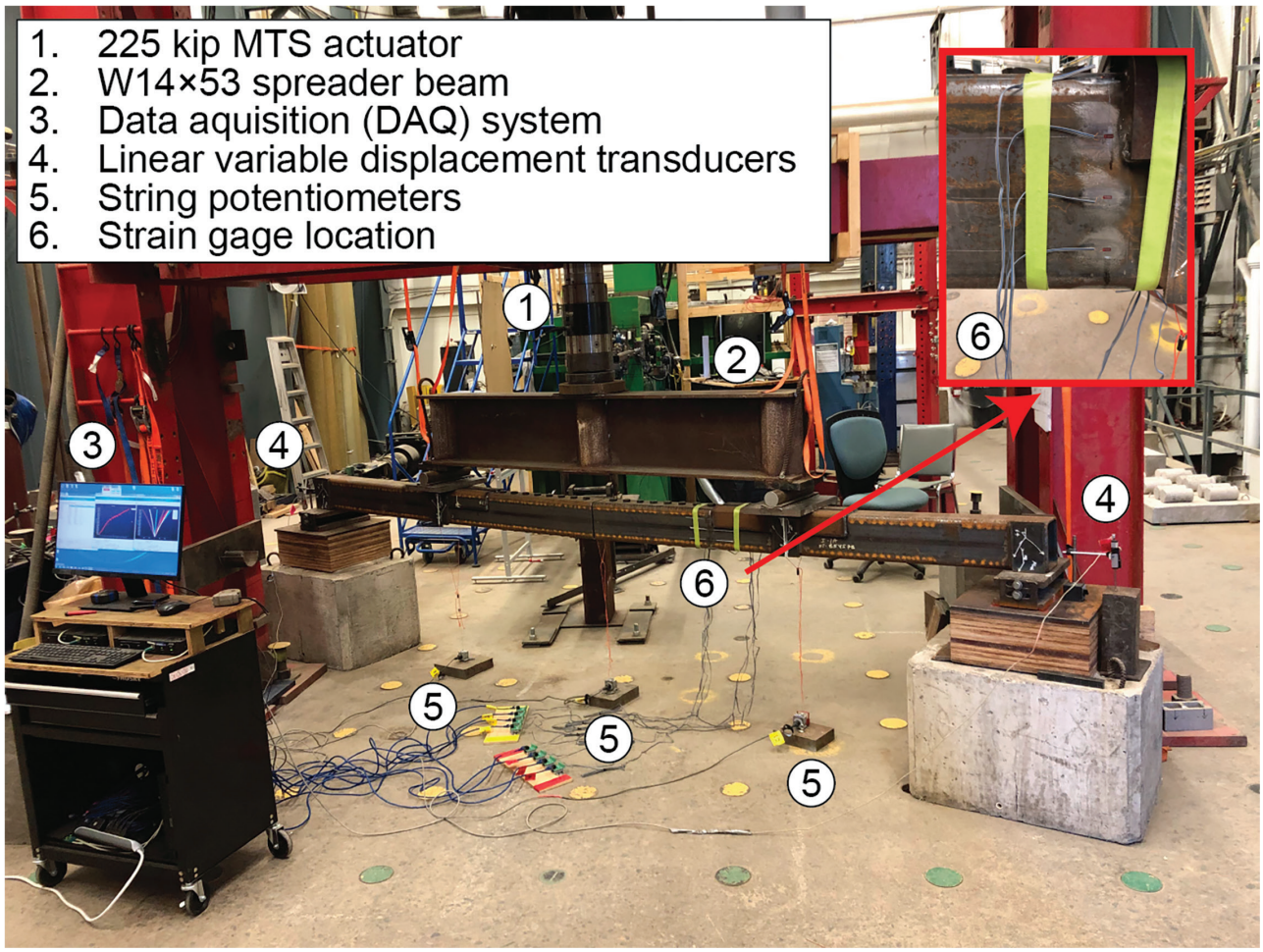

Fig. 6. Instrumentation.

(a) Specimen 3 (HSS 7×7×¼)

(b) Specimen 4 (HSS 8×8×½)

(c) Specimen 10 (HSS 12×8×⅜)

(d) Specimen 11 (HSS 7×5×⅜)

Fig. 7. RHS tension flange ruptures.

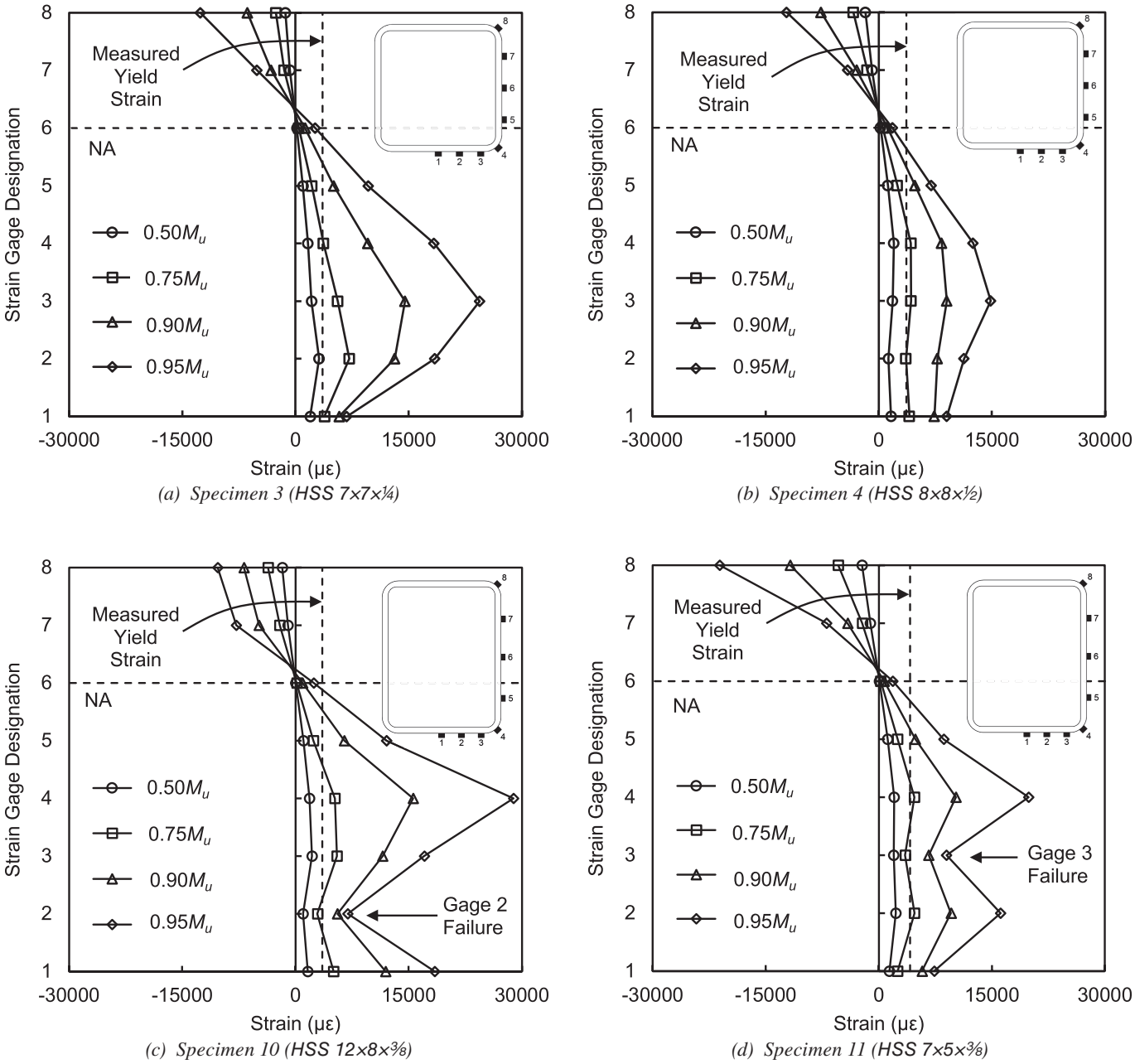

(a) Specimen 3 (HSS 7×7×¼)

(b) Specimen 4 (HSS 8×8×½)

(c) Specimen 10 (HSS 12×8×⅜)

(d) Specimen 11 (HSS 7×5×⅜)

Fig. 8. Measured strains at the critical net section.

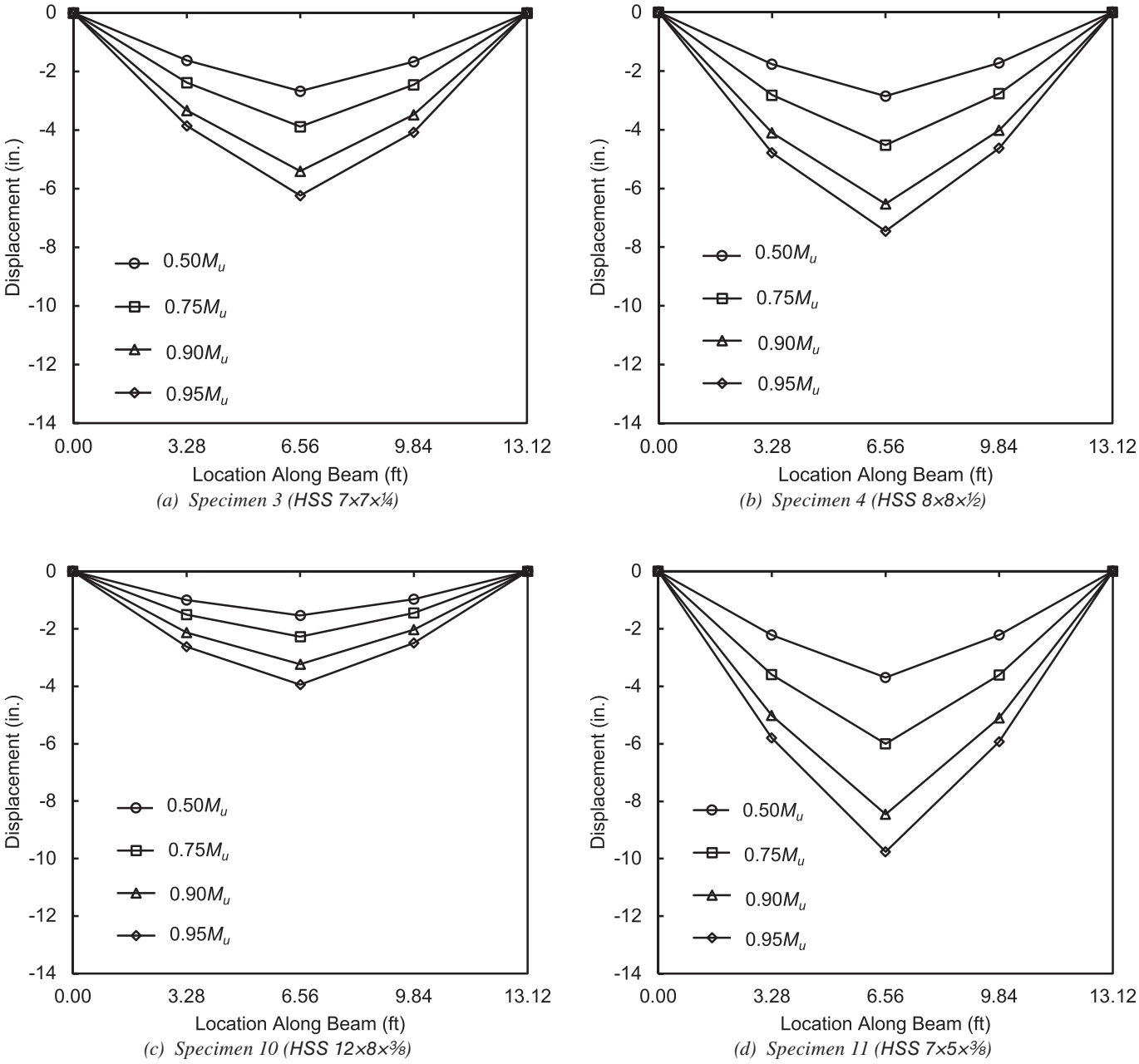

(a) Specimen 3 (HSS 7×7×¼)

(b) Specimen 4 (HSS 8×8×½)

(c) Specimen 10 (HSS 12×8×⅜)

(d) Specimen 11 (HSS 7×5×⅜)

Fig. 9. Beam displacement profiles.

Table 7. Measured and Predicted Nominal Flexural Strength(s)					
		AISC *Specification*		Equation 3	
No.	M_u (kip-ft)	M_n (kip-ft)	M_u/M_n	M_n (kip-ft)	M_u/M_n
1*	57.8	36.9	1.56	51.5	1.12
2*	88.7	74.0	1.20	91.8	0.97
3	99.2	72.2	1.37	90.6	1.10
4	214	157	1.36	188	1.14
5*	167	186	0.90	247	0.68
6*	171	190	0.90	250	0.68
7	318	217	1.47	269	1.18
8	168	101	1.67	157	1.07
9	346	204	1.70	286	1.21
10	331	184	1.80	273	1.21
11	116	64.6	1.79	93.7	1.24
12	117	67.5	1.73	95.4	1.23
Mean			1.45 (1.61)		1.07 (1.17)
CoV			0.211 (0.107)		0.177 (0.049)
* Note: Non-TFR failure modes.					

This, along with the significant amount of tensile strain consistently measured in gage 4, initially suggests that the AISC *Specification*'s current simplified approach to calculating the RHS tension flange area (A_{fg}, and hence, A_{fn}) according to Sections B4.3 and F13.1 (i.e., $b = B\text{-}4t_{des}$, where b is the width of the element) is conservative.

The four remaining specimens (i.e., Specimens 1, 2, 5, and 6) failed due to the manifestation of other limit states. Specimen 1, which was the first to be tested (without compression flange reinforcing) failed by buckling of the compression flange. Specimen 2, which included this reinforcing, failed due to excessive rotation of the connection. This rotation caused the ends of the adjoining RHS members to butt up and yield in compression, which inhibited tension failure on the opposite side. Specimens 5 and 6, which were designed using the "alternate method" (discussed in the section "Design Process for Rupture-Critical Tests"), failed by tensile rupture of the splice plate, as predicted in Table 6. Photos of these failure modes are shown in Figure 10. The peak loads for these specimens (i.e., Specimens 1, 2, 5, and 6) can nonetheless be used as conservative estimates of the tension flange rupture strength.

The ultimate moment, M_u, for each of the 12 specimens (which, for Specimens 3, 4, and 7–12, reflect the true rupture strength of the RHS tension flange) are shown in Table 7, where TFR (in the footnote) stands for tension flange rupture.

ANALYSIS

Evaluation of the AISC *Specification* Nominal Flexural Strength Prediction

The flexural strength, M_n, for each RHS specimen computed using AISC *Specification* Section F13.1 and measured properties is listed in the third column of Table 7 along with the corresponding actual-to-predicted ratios (M_u/M_n). Figure 11(a) shows correlation plots for M_n and M_u and states the mean values of the bias coefficient and coefficient of variation (CoV) for the professional factor, P, (δ_P and V_P, respectively) for (1) all 12 connections (denoted as "all") and (2) for connections that failed by rupture of the tension flange. The conservative estimates (for specimens that failed by other limit states) are indicated by upward arrows in Figure 11(a).

For comparison, the average M_u/M_n ratios and corresponding CoVs from 138 past experiments on tension flange rupture in W-shaped cross-sections are presented in Figure 11(b) for the M_n according to Section F13.1, computed using measured properties. Both numerical results (Carlson et al., 2019) and experimental results from the Georgia Institute of Technology (Schrauben, 1999; Smallidge, 1999; Swanson, 1999; Swanson and Leon, 2000), the University of Texas (Barbaran, 1996; Larson, 1996), the University of Illinois (Schneider and Teeraparbwong, 2002), and the University of California–San Diego (Sato et al., 2007), all of

(a) Specimen 1 (compression flange buckling)

(b) Specimen 2 (flange yielding in compression)

(c) Specimen 5 (tensile rupture of splice plate)

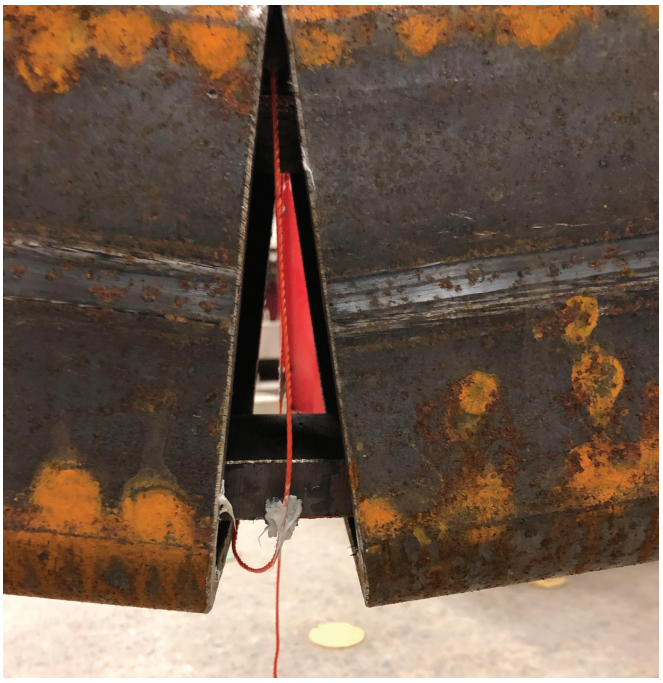

(d) Specimen 6 (tensile rupture of splice plate)

Fig. 10. Additional failure modes.

which were obtained from Swanson (2016) and Arasaratnam (2008), are included.

As shown in Figure 11, Section F13.1 underpredicts the nominal flexural strength of members with holes in their tensile flange (with an actual-to-predicted strength ratio of 1.61 for RHS, 1.65 for all previous data on W-shaped cross sections, and 1.33 for experimentally tested W-shaped cross sections). A contributing factor to the large(r) over-conservatism for RHS when compared to W-shapes is that the ratio of S_x/Z_x is inherently smaller.

The provision can be further assessed by plotting the nominally computed flexural strength normalized by M_p—that is, M_n/M_p—against the ratio A_{fn}/A_{fg}, as shown in Figure 12. In Figure 12(a), the Section F13.1 prediction is shown as a dashed black line for the dual certified ASTM A500 Grades B and C material, and in Figure 12(b), the Section F13.1 prediction is presented as dashed black or red lines for ASTM A572 Grade 50 (2025) or ASTM A992 (2020) and ASTM A36 (2019) material, respectively. Comparing these predictions to the tension flange rupture strengths (M_u/M_p) for each specimen, it is evident that Section F13.1 is a very conservative lower-bound for all (RHS and W-shaped) sections.

Figure 12 also shows that the flexural strength of member(s) with holes in the tension flange indeed depends on the ratio of A_{fn}/A_{fg}, but not as predicted by Equation 2. Figures 13(a) and (b) show the coefficients of determination, R^2, for a linear trendline through the A_{fn}/A_{fg} vs. M_u/M_p ordinates, in which $R^2 = 0.311$ for RHS, given in Figure 13(a), and $R^2 = 0.1697$ for the experimentally tested W-shaped sections, given in Figure 13(b). For all W-shaped specimens (i.e., numerical and experimental), $R^2 = 0.947$, but this is clearly dominated by the finite element (FE) data.

For rupture to manifest in the tensile flange, stresses in the extreme fiber(s) must not only reach F_u, but the material must undergo significant plastic strain (at which point, a plastic flexural stress distribution will develop over the entire net section). This was discussed by Altstadt (2004), who recommended that M_n for members with holes in the tension flange be computed using the net plastic section modulus, Z_n, and the ultimate material strength, F_uZ_n. This was later reinforced in studies by Arasaratnam (2008), Swanson (2016), and Carlson et al. (2019) for W-shaped sections. Figure 13(c) evaluates this approach for the RHS specimens, with Z_n ranging from 8.61 in.^{3} to 47.22 in.^{3} in this study [and Figure 13(d) confirms it for the W-shaped specimens]. The linear trendline for RHS in Figure 13(c) has an R^2 value of 0.967, and for the W-shapes, in Figure 13(d), $R^2 = 0.9592$ for the experiments. When the FE data in Figure 13(d) is also included, R^2 increases to 0.9896.

Recommended Approach

Based on the forgoing analysis, M_n for members (i.e., beams and girders) with holes in the tension flange is best based on the following expression:

$$M_n = F_u Z_n \tag{3}$$

Figure 14(a) shows the correlation between M_u and M_n predicted using Equation 3. The corresponding professional

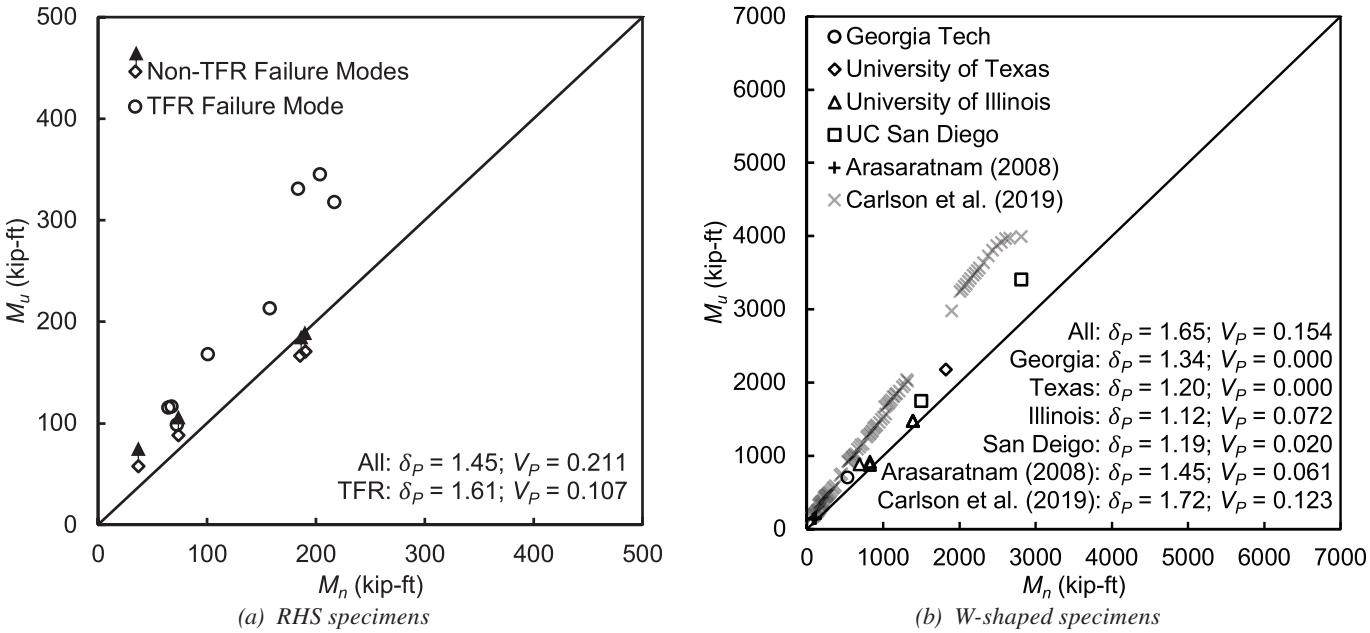

(a) RHS specimens *(b) W-shaped specimens*

Fig. 11. Correlation plots for AISC Specification *Section F13.1.*

factor statistics, δ_P and V_P, are also provided. Figure 14(b) extends this correlation to the W-shaped tests (Arasaratnam, 2008; Barbaran, 1996; Carlson et al., 2019; Larson, 1996; Sato et al., 2007; Schneider and Teeraparbwong, 2002; Schrauben, 1999; Smallidge, 1999; Swanson, 1999; Swanson and Leon, 2000).

Equation 3 is also compared to AISC *Specification* Section F13.1 prediction(s) in Figures 12(a) and 12(b) (as solid lines), shown previously. As shown in these figures and Table 7, Equation 3 is better at predicting the nominal strength (i.e., δ_P closer to unity, by about 44% on average, with a lower CoV) and the observed trends. In Table 7, the means and CoVs are given for the full data set, as well as for the eight specimens that failed by TFR (in parenthesis).

RELIABILITY ANALYSIS

Reliability indices for the foregoing provisions can be computed (and compared) using a first-order reliability method (FORM) analysis (Nowak and Lind, 1979; Schmidt and Bartlett, 2002b) in which

$$\beta = \frac{1}{\sqrt{V_R^2 + V_S^2}} \ln\left[\frac{\delta_R}{\phi}\frac{\alpha_D + \alpha_L\left(L/D\right)}{\delta_D + \delta_L\left(L/D\right)}\right] \tag{4}$$

where β is the reliability index; ϕ is the resistance factor (= 0.9); α_D and α_L are the load factors for dead and live loads, respectively (ASCE, 2022); δ_R, δ_D, and δ_L are the bias coefficients for the resistance, dead load, and live load, respectively; V_R = CoV of δ_R; V_S = CoV of total load effect; and

$$V_s = \frac{\sqrt{\left(\delta_D V_D\right)^2 + \left[\delta_L V_L\left(L/D\right)\right]^2}}{\delta_D + \delta_L\left(L/D\right)} \tag{5}$$

where V_D and V_L = CoVs of δ_D and δ_L, respectively.

This approach is described in Schmidt and Bartlett (2002b) and, in this study, a nondimensional live-to-dead load ratio (L/D) range of $1 \le L/D \le 3$ is considered (Ziemian, 2010). The value(s) of β found using Equation 4, with ASCE/SEI 7-22 (ASCE, 2022) load factors (i.e., $\alpha_D = 1.40$ for dead load only, and $\alpha_D = 1.20$ and $\alpha_L = 1.60$ for dead plus live load), can then be compared to the AISC *Specification* target of 4.0 for connections (AISC, 2022a).

Statistical Parameters

Statistical parameters for the resistance, R, (i.e., δ_R and V_R) were based on the following model:

$$R = GMPd \tag{6}$$

in which G, M, P, and d are the geometric, material, professional, and discretization factors, respectively. If these factors are lognormally distributed and independent, then

$$\delta_R = \delta_G \delta_M \delta_P \delta_d \tag{7}$$

and

$$V_R = \sqrt{V_G{}^2 + V_M{}^2 + V_P{}^2 + V_d{}^2} \tag{8}$$

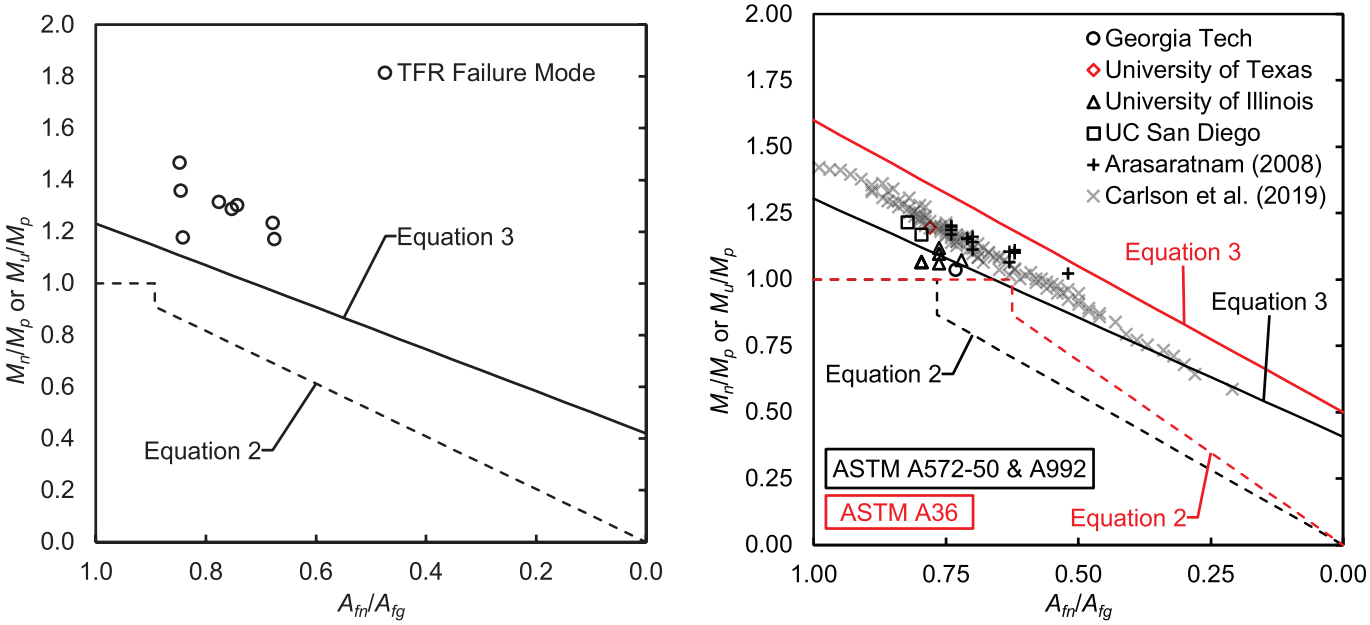

(a) RHS specimens *(b) W-shaped specimens*

Fig. 12. Evaluation of AISC Specification *Section F13.1 and Equation 3.*

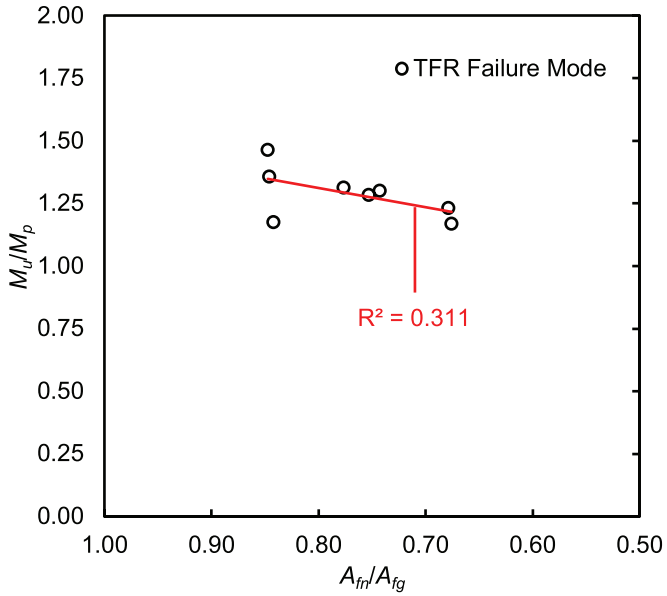

(a) A_{fn}/A_{fg} *vs.* M_u/M_p *for RHS specimens*

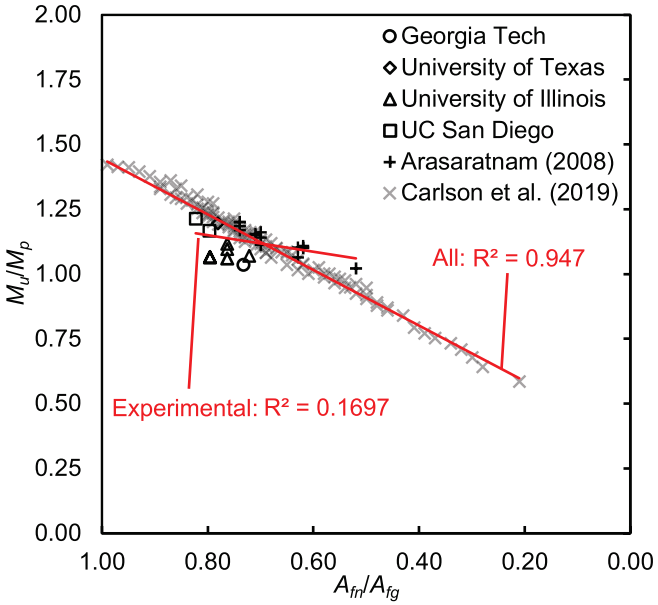

(b) A_{fn}/A_{fg} *vs.* M_u/M_p *for W-shaped specimens*

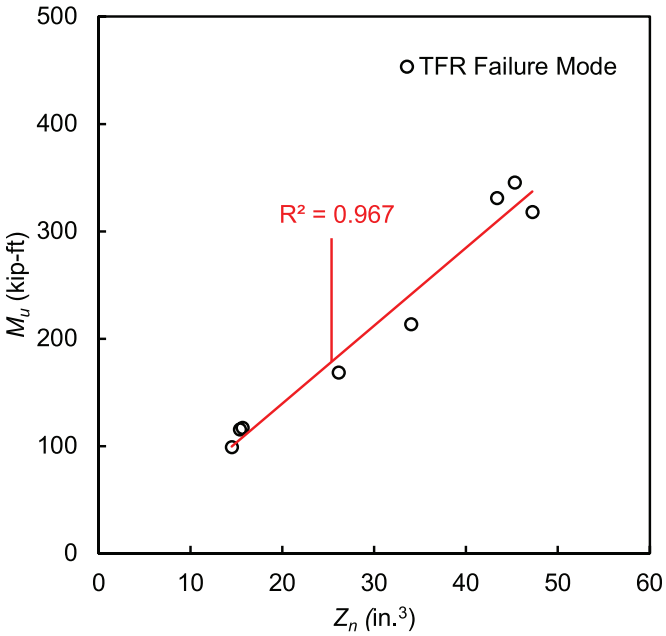

(c) Z_n *vs.* M_u *for RHS specimens*

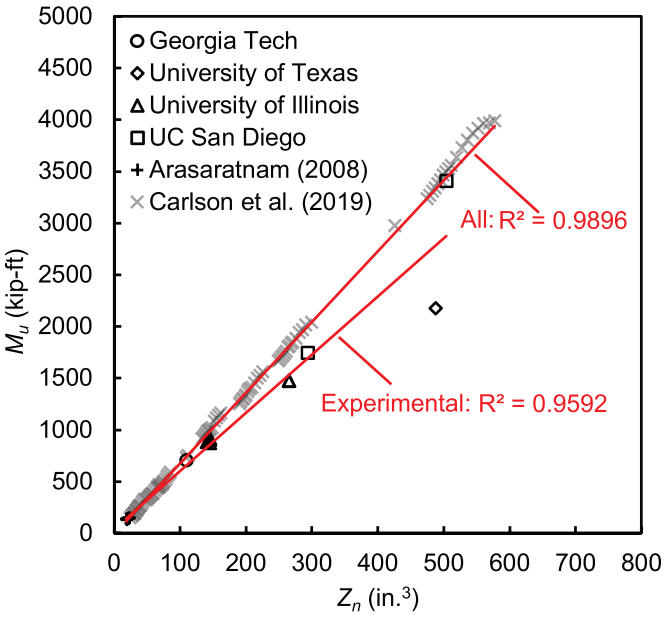

(d) Z_n *vs.* M_u *for W-shaped specimens*

Fig. 13. Assessment of flexural strength dependence on A_{fn}/A_{fg} *and* Z_n.

Table 8. Statistical Parameters for Basic Random Variables		
Variable	**δ**	***V***
B	1.004	0.018
H	1.000	0.010
*t**	0.994	0.007
F_y	1.280	0.090
F_u	1.180	0.080
* Note: Statistics for *t* are with respect to AISC's design wall thickness for ASTM A500 RHS.		

where δ_G, δ_M, and δ_d are the bias coefficients for the geometric, material, and discretization factors, respectively, and V_G, V_M, and V_d are the associated CoVs.

Geometric Factors

For compact RHS that do not satisfy Equation 1, AISC *Specification* Section F13.1 defers to Section F7.1, in which $M_n = M_p = F_yZ$, where Z is the plastic section modulus about the axis of bending. In this case $G = Z$, which can be expressed in terms of B, H, and t. For sections that satisfy Equation 1, M_n is predicted according to the AISC *Specification* using Equation 2, and G is the product of A_{fn}/A_{fg} and S_x, computed for an RHS (with the plastic neutral axis at $H/2$ in the web) as

$$\frac{A_{fn}S_x}{A_{fg}} = \left(1-\frac{n_r d_h}{b}\right)\times \left\{\frac{4\left[\frac{bt^3}{12}+bt\left(\frac{H}{2}-\frac{t}{2}\right)^2\right]+4\left[\frac{th^3}{12}\right]+8\left[0.634t^4+0.75\pi t^2\left(\frac{H}{2}-1.01t\right)^2\right]}{H}\right\} \quad (9)$$

where h = element height = H-4t (AISC, 2022a).

For the recommended approach using Equation 3, $G = Z_n$, computed as

$$Z_n = 2A_{net}\bar{x} \quad (10)$$

in which

$$A_{net} = t\left(b+h+1.5\pi t-n_r d_h\right) \quad (11)$$

and

$$\bar{x} = \frac{\left[0.5t(b-n_r d_h)(H-t)\right]+\left[\left(\frac{h}{2}\right)(2t)\left(\frac{h}{4}\right)\right]+\left[(1.5\pi t^2)\left(\frac{H}{2}-1.01t\right)\right]}{\left[t(b-n_r d_h)\right]+\left[\left(\frac{h}{2}\right)(2t)\right]+\left[1.5\pi t^2\right]} \quad (12)$$

where $\bar{x}$ is the distance between the centroid of A_{net} and the plastic neutral axis.

The statistical parameters for G for each provision were derived for RHS using the statistics for the basic random variables (B, H, and t) (Table 8) (Ncube and Tousignant, 2024), based on

$$\bar{\delta} = \frac{1}{n}\left[\sum_{i=1}^{n}(\delta_i)\right] \quad (13)$$

and

$$V = \frac{1}{\bar{\delta}_i}\sqrt{\frac{1}{n}\left[\sum_{i=1}^{n}(V_i\delta_i)^2+\sum_{i=1}^{n}\left(\bar{\delta_i}-\delta_i\right)^2\right]} \quad (14)$$

where $\bar{\delta}$ is the overall mean bias coefficient value, δ_i = bias coefficient value for an individual shape, V is the coefficient of variation, V_i is the coefficient of variation for an individual shape, and n is the number of specimens.

Using the data in Table 8 for the basic random variables, adopted from Ncube and Tousignant (2024), and considering an outside corner radius of 2.0t (AISC, 2022a), δ_G and V_G were calculated individually for the eight RHS shapes that exhibited tension flange rupture as follows:

$$\delta_G = \frac{G_m}{G_{des}} \quad (15)$$

and

$$V_G^2 = \frac{1}{G_m^2}\Sigma\left[\left(\frac{\partial G_m}{\partial j}\right)\sigma_j\right]^2 \quad (16)$$

where G_m is the mean value of G, G_{des} is the design value of G, j is the random variable(s) comprising G, and σ_j is the standard deviation of the random variable(s) j.

Material Factors

For compact RHS that do not satisfy Equation 1, $M = F_y$ according to the AISC *Specification*. When Equation 1 is satisfied, and for the recommended approach (Equation 3), $M = F_u$. The statistical parameters for F_y and F_u were computed by Ncube and Tousignant (2024) from the results of

Liu (2016). The data shown represents RHS made to the dual certified ASTM A500 in Grades B and C (ASTM, 2021).

Discretization Factor and Load Effects

The statistical parameters for dead and live load effects were taken as $\delta_D = 1.05$, $V_D = 0.100$ and $\delta_L = 0.78$, $V_L = 0.320$, respectively, and the discretization factor was taken as $\delta_d = 1.04$ and $V_d = 0.028$ (Schmidt and Bartlett, 2002a).

FORM ANALYSIS RESULTS

The mean bias coefficient and CoV of the geometric factor for Section F13.1 were found to be $\delta_G = 0.997$ and $V_G = 0.037$, and the professional factor statistics ($\delta_P = 1.61$ and $V_P = 0.107$) are as shown in Figure 11(a) for the specimens failing by TFR only. The mean bias coefficient and CoV of the geometric factor for Equation 3 were found to be $\delta_G = 0.997$ and $V_G = 0.016$, with the professional factor statistics ($\delta_P = 1.17$ and $V_P = 0.049$) shown in Figure 14(a), for the specimens failing by TFR only. By combining these statistics with those of the material and discretization factors, in accordance with Equations 7 and 8, the bias factor and CoV for R can be determined. For Section F13.1, $\delta_R = 2.14$ with $V_R = 0.147$, and for Equation 3, $\delta_R = 1.43$ with $V_R = 0.099$.

To assess the inherent reliability of AISC *Specification* Section F13.1 for W-shape sections, values of δ_G, δ_M, $\delta_d = 1.01$, 1.11, 1.05, respectively, and V_G, V_M, $V_d = 0.035$, 0.063, 0.035, respectively, were adopted from Schmidt and Bartlett (2002a). Similarly, to assess Equation 3, values of δ_G, δ_M, $\delta_d = 1.01$, 1.13, 1.05, respectively, and V_G, V_M, $V_d = 0.034$, 0.044, 0.035, respectively, are used (Schmidt and Bartlett, 2002a), resulting in $\delta_R = 1.93$ and $V_R = 0.173$ for Section F13.1 and $\delta_R = 1.29$ and $V_R = 0.076$ for Equation 3 for all data. For experimentally tested W-shapes, $\delta_R = 1.56$ and 1.24 and $V_R = 0.149$ and 0.084 for Section F13.1 and Equation 3, respectively.

Ranges of β computed from Equation 4, with $\phi = 0.90$, are shown in Figure 15 for both the Section F13.1 provision and Equation 3. In Figure 15, the dashed horizontal line corresponds to the target safety index of $\beta = 4.0$ as outlined in AISC *Specification* Chapter B. The vertical line represents the lower bound of $L/D = 1.0$ considered for this study (Ziemian, 2010). As shown, values of β computed for both Section F13.1—that is, Figures 15(a) and 15(b)—and Equation 3—that is, Figures 15(c) and 15(d)—are at or above the target across the full range of $1 \le L/D \le 3$ for both RHS and W-shaped sections. The high safety indices for Section F13.1 are due almost exclusively to over-conservatism in the current design model.

CONCLUSION

The scope of testing presented herein covered 12 rectangular hollow section (RHS)-to-RHS splice connections loaded under monotonic four-point bending (about their strong axis) to produce tension flange rupture. Each RHS was dual certified to ASTM A500 Grades B and C with an aspect

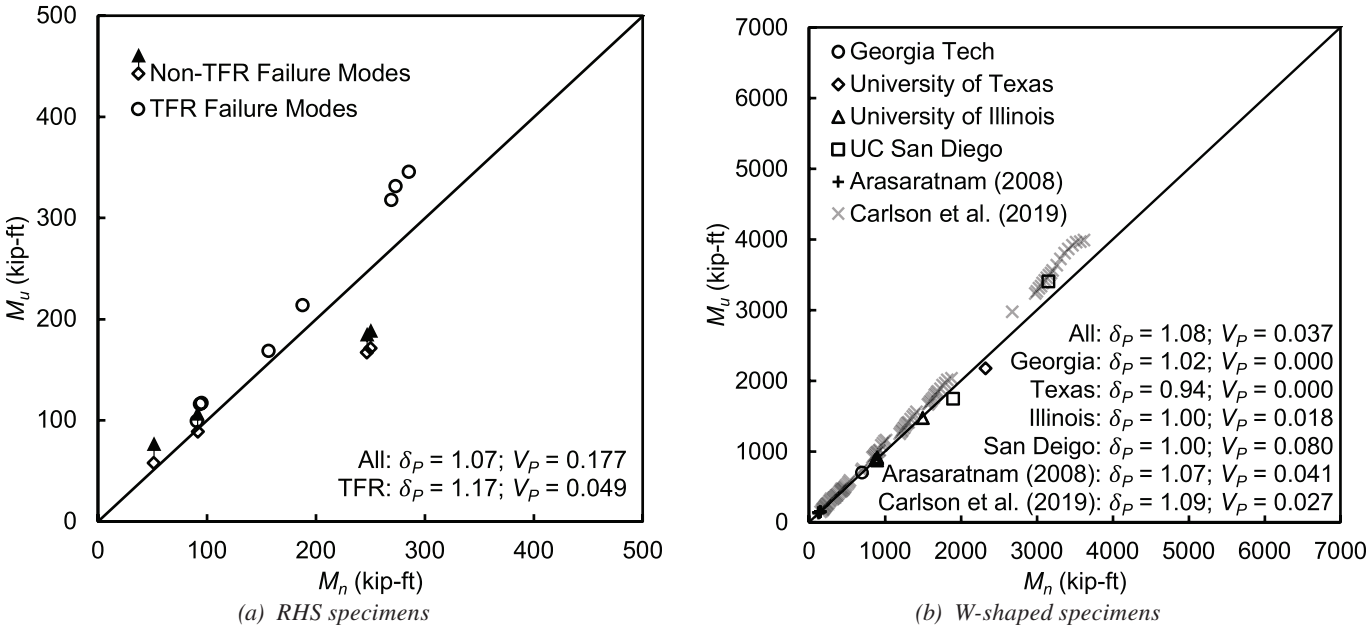

(a) RHS specimens *(b) W-shaped specimens*

Fig. 14. Correlation plots for Equation 3.

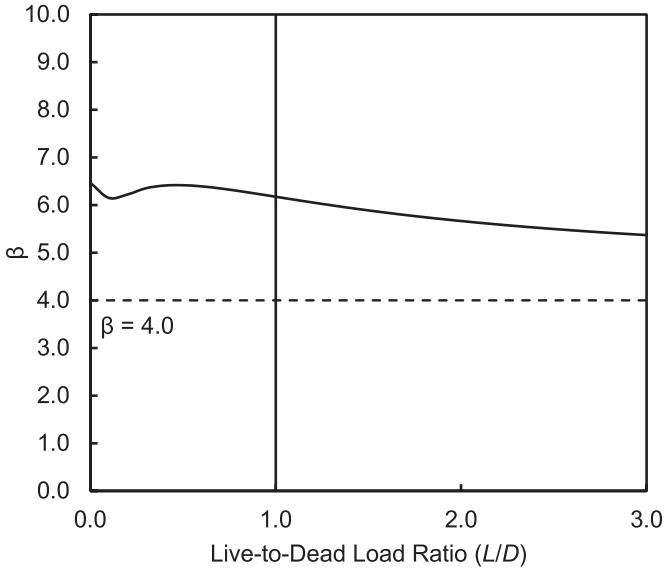

(a) AISC Specification *Section F13.1 for RHS specimens*

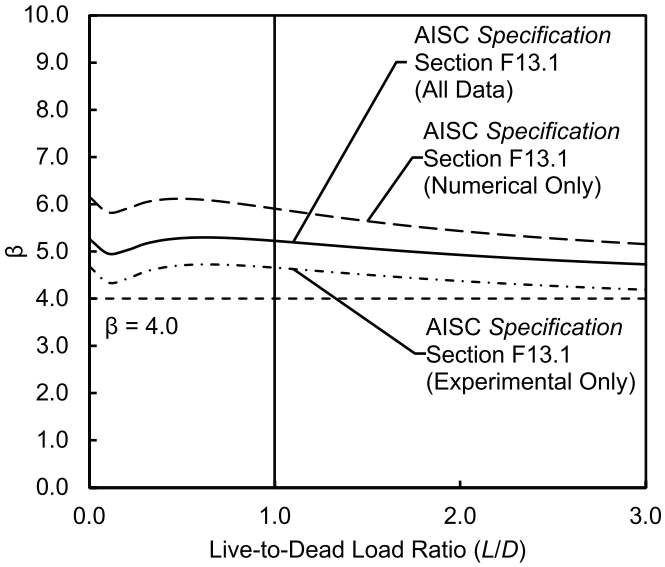

(b) AISC Specification *Section F13.1 for W-shaped specimens*

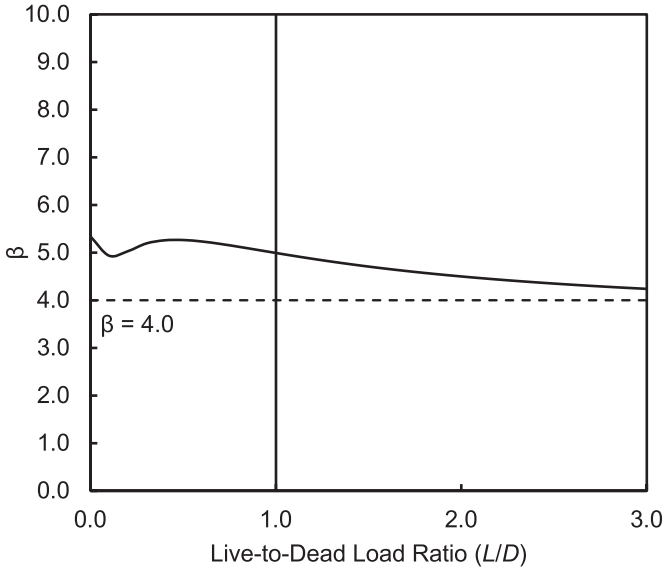

(c) Equation 3 for RHS specimens

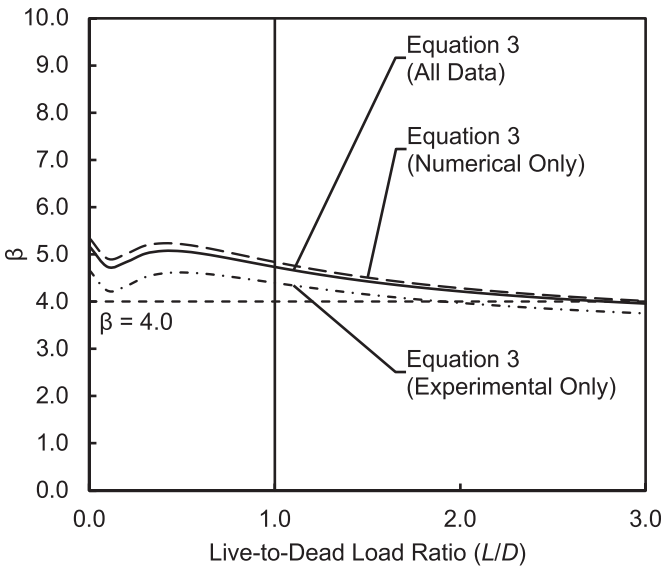

(d) Equation 3 for W-shaped specimens

Fig. 15. β *versus* L/D *for AISC* Specification *Section F13.1 and Equation 3.*

ratio(s) of 1.0 to 2.0, nominal wall thickness(es) from ¼ in. to ⅝ in., a flange slenderness ratio(s) from 10.03 to 25.16, and a web slenderness ratio(s) from 10.03 to 48.71. Each connection had a net plastic section modulus ranging from 8.61 in.^{3} to 47.22 in.^{3} and either a one- or two-row bolt configuration. Based on these results, and an analysis of 138 previous tests on W-shaped sections (113 numerical and 25 experimental), which were primarily comprised of ASTM A992 and A572-50 material, it can be concluded that:

- AISC *Specification* Section F13.1 predictions of M_n for members with holes in their tension flange are over-conservative.
- The flexural strength of members with holes in their tension flange is well-correlated with Z_n, and less so with the ratio of A_{fn}/A_{fg}.
- The nominal strength equation given by Equation 3, which utilizes Z_n and F_u, provides a significant improvement in accuracy over AISC *Specification* Section F13.1, while still providing acceptable levels of reliability.

It is therefore recommended that the latter half of AISC *Specification* Section F13.1 be modified to:

F13. PROPORTIONS OF BEAMS AND GIRDERS

1. Strength Reductions for Members with Bolt Holes in the Tension Flange

In addition to the limit states specified in other sections of this chapter, the nominal flexural strength, M_n, shall be limited according to the limit state of tensile rupture of the tension flange.

$$M_n = F_u Z_n \quad \text{(F13-1)}$$

where

Z_n = minimum net plastic section modulus, in.^{3} (mm^3)

F_u = specified minimum tensile strength, ksi (MPa)

ACKNOWLEDGMENTS

The authors of this paper gratefully acknowledge the financial support of the Canadian Institute of Steel Construction (CISC) and the Natural Sciences of Engineering Research Council (NSERC). The authors also wish to acknowledge Atlas Tube for supplying the steel rectangular hollow sections and Cherubini Metal Works for their fabrication services.

SYMBOLS

A_{fg} Gross area of tension flange, in.^{2}

A_{fn} Net area of tension flange, in.^{2}

A_{gc} Gross area subjected to compression, in.^{2}

A_{gv} Gross area subjected to shear, in.^{2}

A_{net} Net-effective area subjected to tension under pure flexure, in.^{2}

A_{nt} Net area subjected to tension, in.^{2}

A_{nv} Net area subjected to shear, in.^{2}

B Overall width, in.

B_p Splice plate overall width, in.

B_s Stiffener plate overall width, in.

E Modulus of elasticity, ksi

F_{nv} Nominal shear stress of the bolt, ksi

F_u Specified minimum tensile strength, ksi

F_y Specified minimum yield strength, ksi

G Geometric factor

G_{des} Design value of the geometric factor

G_m Mean value of the geometric factor

H Overall height, in.

H_s Stiffener plate overall height, in.

L Overall beam length, in.

M Material factor

M_a Applied moment, kip-ft

M_n Nominal flexural strength, kip-ft

M_p Plastic moment, kip-ft

M_u Ultimate moment, kip-ft

P Professional factor

R Resistance factor

R^2 Coefficient of determination

S_n Minimum net elastic section modulus taken about the axis of bending, in.^{3}

S_x Minimum elastic section modulus taken about the x-axis, in.^{3}

V Coefficient of variation

V_D Coefficient of variation of the dead load

V_d Coefficient of variation of the discretization factor

V_G Coefficient of variation of the geometric factor

V_i Coefficient of variation for an individual shape

V_L Coefficient of variation of the live load

V_M Coefficient of variation of the material factor

V_P Coefficient of variation of the professional factor

V_R Coefficient of variation of the resistance factor

V_S Coefficient of variation of the total load effect

Y_t Coefficient corresponding to yield-to-tensile strength ratio

Z Plastic section modulus taken about the axis of bending, in.^{3}

Z_x Plastic section modulus taken about the x-axis, in.^{3}

Z_n Net plastic section modulus taken about the axis of bending, in.^{3}

b Width of the element, in.

d Discretization factor

d Nominal diameter of fastener, in.

d_h Diameter of bolt hole, in.

g Transverse center-to-center spacing between fastener gage lines, in.

h Height of the element, in.

j Random variable(s) comprising the geometric factor expression

l_{bolt} Nominal bolt length, in.

l_c Clear distance, in the direction of the force, between the edge of the hole and the edge of the adjacent hole or edge of material, in.

n Number of specimens

n_b Number of bolts per connection

n_r Number of bolts per row

s Longitudinal center-to-center spacing of any two consecutive bolt holes, in.

t Measured wall thickness, in.

t_{des} Design wall thickness, in.

t_{nom} Nominal wall thickness, in.

t_p Splice plate thickness, in.

t_s Stiffener plate thickness, in.

$\bar{x}$ Distance between the centroid of net-effective area subjected to tension and the plastic neutral axis, in.

y Geometric centroid, in.

α_D Load factor for dead load

α_L Load factor for live load

β Reliability index

$\bar{\delta}$ Overall mean bias coefficient value

δ_D Bias coefficient of the dead load

δ_d Bias coefficient of the discretization factor

δ_G Bias coefficient of the geometric factor

δ_i Bias coefficient value for an individual shape

δ_L Bias coefficient of the live load

δ_M Bias coefficient of the material factor

δ_P Bias coefficient of the professional factor

δ_R Bias coefficient of the resistance factor

ε_r Strain at rupture, in./in.

ε_u Strain at the ultimate stress, in./in.

ε_y Strain at the yield stress, in./in.

σ_j Standard deviation of the random variable(s) comprising the geometric factor expression

ϕ Resistance factor

REFERENCES

AISC (2022a), *Specification for Structural Steel Buildings*, ANSI/AISC 360-22, American Institute of Steel Construction, Chicago, Ill.

AISC (2022b), *Seismic Provisions for Structural Steel Buildings*, ANSI/AISC 341-22, American Institute of Steel Construction, Chicago, Ill.

AISC (2023), *Steel Construction Manual*, 16th Ed., American Institute of Steel Construction, Chicago, Ill.

Altstadt, S. (2004), "Tensile Strength and Ductility of High Performance Steel Girders," M.S. Thesis, University of Minnesota, Minneapolis, Minnesota.

Arasaratnam, P. (2008), "Effects of Flange Holes on Flexural Behavior of Steel Beams," M.A.Sc. Thesis, Department of Civil Engineering, McMaster University, Hamilton, Ontario.

ASCE (2022), *Minimum Design Loads and Associated Criteria for Buildings and Other Structures*, ASCE/SEI 7-22, American Society for Civil Engineers, Reston, Va.

ASTM (2019), *Standard Specification for Carbon Structural Steel*, A36/A36M, American Society for Testing and Materials International, West Conshohocken, Pa.

ASTM (2020), *Standard Specification for Structural Steel Shapes*, A992/A992M, American Society for Testing and Materials International, West Conshohocken, Pa.

ASTM (2021), *Standard Specification for Cold-Formed Welded and Seamless Carbon Steel Structural Tubing in Rounds and Shapes*, A500/A500M-21, American Society for Testing and Materials International, West Conshohocken, Pa.

ASTM (2022), *Standard Test Methods for Tension Testing of Metallic Materials*, ASTM E8/E8M-22, American Society for Testing and Materials International, West Conshohocken, Pa.

ASTM (2023), *Standard Specification for High Strength Structural Bolts and Assemblies, Steel and Alloy Steel, Heat Treated, Inch Dimensions 120 ksi and 150 ksi Minimum Tensile Strength, and Metric Dimensions 830 MPa and 1040 MPa Minimum Tensile Strength*, ASTM F3125/F3125M, American Society for Testing and Materials International, West Conshohocken, Pa.

ASTM (2025), *Standard Specification for High-Strength Low-Alloy Columbium-Vanadium Structural Steel*, A572/A572M, American Society for Testing and Materials International, West Conshohocken, Pa.

Barbaran, F.V.U. (1996), "Tension Bolt Behavior in Moment Connections for Seismic Applications," M.S. Thesis, Department of Civil, Architectural, and Environmental Engineering, University of Texas at Austin, Austin, Texas.

Carlson, R.B., Swanson, J.A., Rassati, G.A., and Burns, T.M. (2019), "Flexural Strength of Steel Beams with Holes in the Tension Flange," Internal Report, Department of Civil and Environmental Engineering, University of Cincinnati, Cincinnati, Ohio.

CSA (2023), *General Requirements for Rolled or Welded Structural Quality Steel/Structural Quality Steel*, CSA G40.20-13/G40.21-13 (R2023), Canadian Standards Association, Toronto, Ontario.

Dexter, R.J. and Altstadt, S.A. (2004), "Strength and Ductility of Tension Flange Girders," *Recent Developments in Bridge Engineering*, *Proceedings of the Second New York City Bridge Conference*, October 20–21, 2003, New York, N.Y., Mahmoud, K.M. (ed.), A.A. Balkema/Swets & Zeitlinger, Lisse, The Netherlands, pp. 67–81.

Larson, P.C. (1996), "The Design and Behavior of Bolted Beam-to-Column Frame Connections under Cyclical Loading," M.S. Thesis, Department of Civil, Architectural, and Environmental Engineering, University of Texas at Austin, Austin, Texas.

Liu, J. (2016), "Updates to Expected Yield Stress and Tensile Stress Ratios for Determination of Expected Member Capacity in the 2016 AISC Seismic Provisions," *Engineering Journal*, AISC, Vol. 53, No. 4, pp. 215–228.

Ncube, M. and Tousignant, K. (2024), "Assessing the Impact of Design Wall Thickness on the Reliability of ASTM A500 HSS Compression Members," *Proceedings of the Annual Conference of the Canadian Society of Civil Engineering*, July 5–7, Niagara Falls, Ontario.

Nowak, A.S. and Lind, N.C. (1979), "Practical Bridge Code Calibration," Journal of the Structural Division, ASCE, Vol. 105, No. 12, pp. 2497–2510.

Sato, A., Newell, J., and Uang, C.M. (2007), "Cyclic Testing of Bolted Flange Plate Steel Moment Connections for Special Moment Frames," Final Report to the American Institute of Steel Construction from the Department of Structural Engineering, University of California, San Diego.

Schmidt, B.J. and Bartlett, F.M. (2002a), "Review of Resistance Factor for Steel: Data Collection," *Canadian Journal of Civil Engineering*, Vol. 29, No. 1, pp. 98–108.

Schmidt, B.J. and Bartlett, F.M. (2002b), "Review of Resistance Factor for Steel: Resistance Distributions and Resistance Factor Calibration," *Canadian Journal of Civil Engineering*, Vol. 29, No. 1, pp. 109–118.

Schneider, S.P. and Teeraparbwong, I. (2002), "Inelastic Behavior of Bolted Flange Plate Connections," *Journal of Structural Engineering*, ASCE, Vol. 128, No. 4, pp. 492–500.

Schrauben, C.S. (1999), "Behavior of Full-Scale Bolted Beam-to-Column T-Stub and Clip Angle Connections under Cyclic Loads," M.S. Thesis, submitted to the faculty of the Georgia Institute of Technology, Atlanta, Georgia.

Smallidge, J.M. (1999), "Behavior of Bolted Beam-to-Column T-Stub Connections under Cyclic Loading," M.S. Thesis, submitted to the faculty of the Georgia Institute of Technology, Atlanta, Georgia.

Swanson, J.A. (1999), "Characterization of the Strength, Stiffness, and Ductility of T-Stub Connections," Ph.D. dissertation, Georgia Institute of Technology, Atlanta, Georgia.

Swanson, J.A. (2016), "Strength of Beams in Beam-to-Column Connections with Holes in the Tension Flange," *Engineering Journal*, AISC, Vol. 53, pp. 159–172.

Swanson, J.A. and Leon, R.T. (2000), "Bolted Steel Connections: Tests on T-Stub Components," *Journal of Structural Engineering*, ASCE, Vol. 126, No. 1, pp. 50–56.

Yuan, Q., Swanson, J., and Rassati, G.A. (2004), "An Investigation of Hole Making Practices in the Fabrication of Structural Steel," Internal Report, Department of Civil and Environmental Engineering, University of Cincinnati, Cincinnati, Ohio.

Ziemian, R.D. (2010), *Guide to Stability Design Criteria for Metal Structures*, 6th Ed., Wiley, N.Y.